23rd Topical Conference on Radiofrequency Power in Plasmas (RFPPC 2019), Hefei, China, May 14-17, 2019. To appear in AIP Conference Proceedings.

A Comparison of RF Heating Calculated with the CQL3D Fokker-Planck Solver and with a Monte-Carlo Code

Yu. V. Petrov[1, a)] and R. W. Harvey[1, b)]

[1]*CompX, Del Mar, California 92014 USA*

[a)]Corresponding author: petrov@compxco.com
[b)]rwharvey@compxco.com

Abstract. The bounce-average finite-difference Fokker-Planck code CQL3D [1] is an established tool for modeling of RF and NBI heating. Recently it has been augmented with a Finite-Orbit-Width (FOW) treatment of ions [2]. For validation purposes, and also for accessing the high-collisionality regime, and toroidal variation effects, a Monte-Carlo particle code RFMC has been developed that is based on the MCGO code [3]. Among other goals is an accurate calculation of ion and neutral particle losses to a realistic vacuum chamber. Ion orbits from a thermal initial distribution, and/or from an NBI source, are integrated in time including the effects of collisions, charge exchange events and RF kicks. The RF kicks are based on local quasilinear diffusion coefficients that include all components of RF electric field and all-orders terms for finite Larmor radius effects. The RF operator acts on both perpendicular and parallel component of particle momentum. A procedure for accumulation of particle loss distributions to the wall for test ions and neutrals, is included as a function of poloidal and toroidal distance along the wall, particle energy and the incident angle. As a verification study, a comparison is made between CQL3D and the RFMC code for scenarios of minority ICRH in C-Mod. The calculated profiles of RF power deposition are very similar in CQL3D and RFMC runs, the distribution functions also agree in the main features of non-Maxwellian tails, although some details are different. We also find good agreement of the NBI heating in NSTX, including FOW effects.

1 INTRODUCTION

Among the computational tools for description of RF and NBI heating of plasmas, the bounce-average finite-difference Fokker-Planck code CQL3D [1] is in an active phase of usage and development, with recently added functionalities such as the Finite-Orbit-Width treatment of ions [2] and implementation of Ampere-Faraday equations for calculation of time-dependent toroidal electric field evolution [4]. A known limitation for bounce-average codes is the assumption of toroidal symmetry, which can only provide a toroidally averaged calculation of particle deposition to plasma facing components. Mostly for this specific purpose of accurate calculation of particle loss spectra to a realistic chamber wall with 3D structures (RF antennas, ports, limiters), we reactivated and upgraded a Monte-Carlo code, which we designate RFMC. It is based on MCGO code [3] that has been developed in mid-80's and was used to confirm acceptable wall heat loading in DIII-D. Also, as another advantage, it can access a high-collisionality regime, and also serve as a verification/validation tool for CQL3D.

In RFMC, the guiding center orbits are followed including effects of Coulomb collisions, RF kicks and charge-exchange (CX) events with background cold neutrals. A fast ion (FI) may undergo several CX events from ionized to neutral and back to ionized state before it reaches the wall. Coulomb collisions of test particles with thermalized species include pitch angle scattering, slowing down and diffusion in energy, using the tabulated background plasma profiles. Collisions can be accelerated ("goosed") for a faster slowing down in energy. Equilibrium magnetic field is imported from eqdsk data. The initial loading may include a Maxwellian group of particles and/or NBI-produced source of FIs; the latter is generated by FREYA module – similar to one used in CQL3D. During a run, the velocity distribution function is formed at the midplane radial bins. Also, the radial profiles, such as flux-surface-average density or current, are constructed based on the accumulated time that particles spend in each flux surface bin.

When the particle reaches the wall, it is accumulated onto a 4D grid, – as a function of poloidal and toroidal distance along the wall, particle energy and the incident angle. This is done separately for ions and fast neutrals. The initial results, with a toroidally symmetric wall, are demonstrated in Fig. 1.

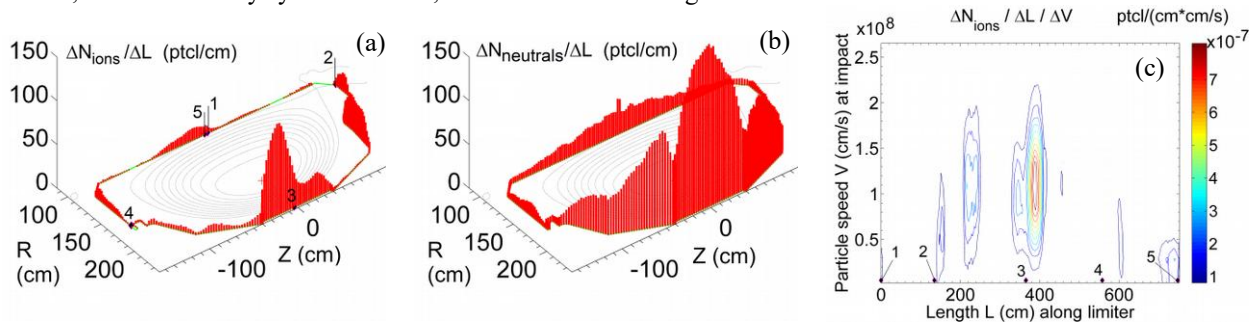

FIGURE 1. Count of (a) ions, and (b) neutrals that hit the wall, per unit length along limiter (summed over all toroidal angles at impact). Also, (c) shows the distribution of ions that hit the wall (limiter), per unit length along limiter and unit speed, as a function of speed at impact and the length along limiter in (*R,Z*) plane; the initial 4D data is reduced by summing over all incident angles and toroidal angles at impact. The points marked "1" through "5" are the same as those in panel (a).

In this example 3 million particles are started in DIIID as NBI-born D^+ ions at initial energies 70, 35 and 23.3 keV. Also a group of 3000 thermalized ions is added. The fast ions are followed until they reach a fraction of ion thermal energy (0.2-3.2 keV depending on radius), or they hit the wall, or by ion charge-exchanging to a neutral and then hitting the wall. The next step is to use a realistic wall, which is a challenging task because of memory constraints. It will be a focus of the further development of RFMC. Here, the main subject is the RF or NBI heating of plasma, which we discuss in the next two sections.

2 RF OPERATOR AND TESTS FOR ICRH

The RF kick operator is a recent addition to RFMC, and it includes several versions. One of them is the straight-forward integration of the particle force equation for the perpendicular component of velocity in a given RF field [5]. However, this approach requires a very small time step – a fraction of a gyro-period, – because of a quickly oscillating kernel of the integral, $\exp\left(-i\left(\omega-\Omega_c\right)t\right)$, especially away from the cyclotron resonance. One way to overcome this constraint is to evaluate the overall gain in $V_\perp$ as the particle goes through resonance, by expanding $\Omega_c(t)$ around the resonance [5]. This is implemented as a second version in the code. Of course, in this version, the finite Larmor radius effects are lost, so, – there is no interaction with high-harmonic resonances. Last, the third implemented version is based on knowledge of local quasi-linear RF diffusion coefficients. The derivation is done in analogy with a general consideration of the collision operator [6], and inspired by recent efforts made for the NUBEAM RF operator [7, 8]. The kicks in perpendicular and parallel components of particle velocity are

$$\Delta\left(V_\perp^2\right)=\left(v_{s\perp}V^2\right)\Delta t+2\sqrt{3}\left(R_s-0.5\right)\sqrt{\left(8D_\perp V_\perp^2\Delta t\right)}\ , \quad (1)$$

$$\Delta\left(V_\parallel\right)=\left(v_{s\parallel}V_\parallel\right)\Delta t+2\sqrt{3}\left(R_s-0.5\right)\sqrt{\left(2D_\parallel\Delta t\right)}\ , \quad (2)$$

where $\left(v_{s\perp}V^2\right)=\dfrac{\partial\left(4D_\perp V_\perp^2\right)}{\partial\left(V_\perp^2\right)}+\dfrac{\partial\left(2D_{\parallel\perp}V_\perp\right)}{\partial\left(V_\parallel\right)}$ and $\left(v_{s\parallel}V_\parallel\right)=\dfrac{\partial D_{\parallel\perp}}{\partial V_\perp}+\dfrac{\partial D_\parallel}{\partial V_\parallel}+\dfrac{D_{\parallel\perp}}{V_\perp}$

$$D_{\parallel\perp}=\sqrt{D_\parallel D_\perp} \quad (3)$$

The local QL diffusion coefficients $D_\perp$, $D_\parallel$ and include all components of RF electric field (E_+, E_-, $E_\parallel$) and Bessel functions J_{n-1} , J_{n+1} , J_n of argument $k_\perp\rho_{Larm}$ [5]. Note that Eqs.(1-2) contain one random number R_s (from uniform distribution in [0;1)), while the Coulomb operator [6] contains two independent numbers.

The kicks are applied at several time steps before and after the resonance crossing, within effective wave-particle interaction time [9, 10]. It has been verified that the results are almost independent on the orbital time step Δt, – with smaller Δt, there are more kicks around the resonance, but they have smaller magnitude.

For verification, we compared the results from CQL3D and RFMC for the case of minority H^+ heating in C-Mod, with H(10%)+D(90%) mixture [11]. Both codes were run in zero-orbit-width (ZOW) mode for this test. In RFMC, a special option was applied zeroing the particle drift normal to flux surfaces. The Fast wave propagation was calculated by AORSA; however, CQL3D runs were only using the QL diffusion coefficients calculated by AORSA, while RFMC was importing the RF electric field components, and forming the QL diffusion coefficients internally. In AORSA calculations, four toroidal modes were used with $N_\phi = \pm 9$ and ± 20; the power deposition is considered to be toroidally symmetric. The example of computed distribution function is shown in Fig. 2.

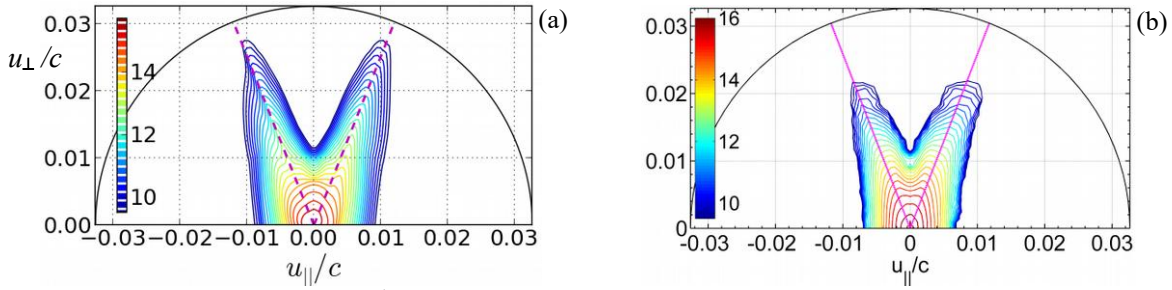

FIGURE 2. Distribution function of H^+ (in log10 scale) computed with (a) CQL3D and (b) RFMC at the midplane radial coordinate R=73cm, not far from the ICR layer that goes through the magnetic axis at R≅68cm. Dashed lines mark the trapped-passing boundary, the semi-circle corresponds to energy 500 keV.

It should be noted that here the distribution functions are not at steady-state. This is especially important for interpretation of results from RFMC (or any MC code) because the data must be accumulated over a long enough time frame. For Fig. 2(b), the distribution was collected over a relatively large time frame t = [0.5; 1.5] ms. In CQL3D, the distribution shown in Fig. 2(a) is the instantaneous solution at t =1.0 ms. In spite of this consideration, the distribution functions show similar features. The dynamics of power deposition and collisional power transfer are shown in Fig. 3. The total RF power coupled to plasma reaches 4.3 MW as computed by CQL3D, or 4.4 MW as computed by RFMC. It is seen that the RF deposition profiles do not change much in time,– because most of the power is deposited to the thermalized part of the H^+ distribution function (which remains almost unchanged) rather than to a less-populated tail (which continues to grow). In contrast, the collisional power transferred from minority H^+ ions to background electrons and ions continues to grow in time,– because the power is transferred from the tail of H^+ species, which is getting more populated in time. The time frames in RFMC over which the data was accumulated are specified in the figure. For CQL3D results the profiles are averaged over corresponding time frames (six time points in each time frame). Based on these initial tests, we conclude that the two codes yield the same main values and dynamics of plasma heating, except for a small disagreement at the plasma edge, which could be due to a different treatment of short-scale IC wave at plasma edge.

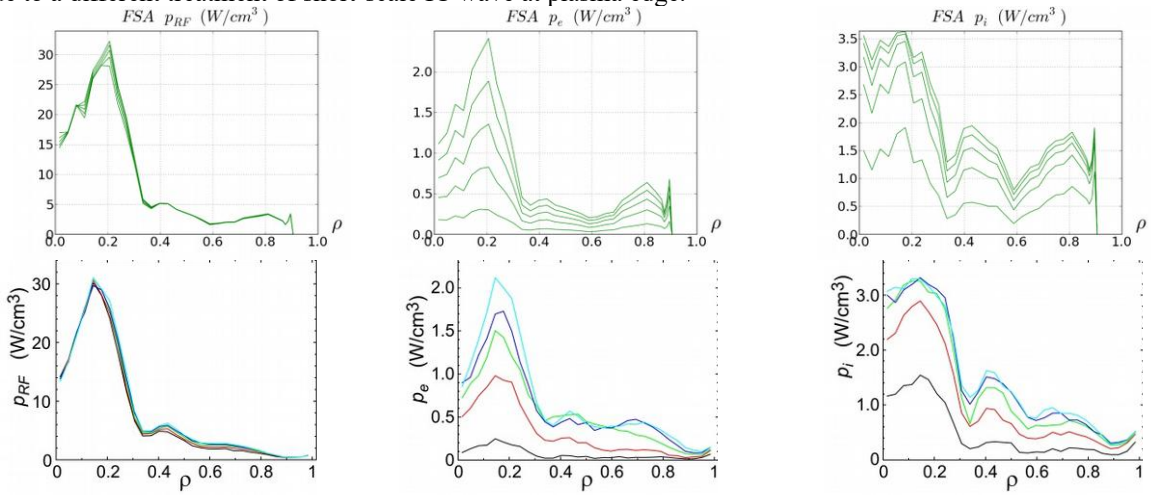

FIGURE 3. First column – RF power deposition profiles to the minority H^+ ions, second column – collisional power transfer from H^+ to background electrons, third column – collisional power transfer from H^+ to background D^+ ions. Upper row is

(a) (b)

calculated by CQL3D, and the lower row is from RFMC. The five curves in each panel correspond to time frames [0; 0.3ms], [0.3ms; 0.6ms], [0.6ms; 0.9ms], [0.9ms; 1.2ms], and [1.2ms; 1.5ms]).

In terms of computational efficiency, the RFMC run was using 1 M test particles (which seems to be sufficient for yielding a smooth distribution function and power profiles), and took 82 sec on 480 MPI cores. This cpu time is approximately 57% larger than in no-RF run, however, we only used four toroidal modes for RF field. In the CQL3D run, only 32 cores were used, and it took 536 sec to compute 30 time steps.

3 NBI HEATING IN NSTX

In the tests discussed above the finite-orbits-width (FOW) effects are negligible because of the strong magnetic field in C-Mod. In fact, a FOW run was made with RFMC, and it showed only a slight broadening of the power transfer profiles, and only at $\rho < 0.2$ where the poloidal magnetic field becomes small. In this regard, the test case of NSTX, especially with NBI-produced fast ions, can serve as a good subject study of FOW effects. In Fig. 4, the examples of distribution functions computed with CQL3D and RFMC are shown for the relaxation of fast ions in NSTX. These are the steady-state distributions at t = 60 ms (the slowing down time is 60 ms in plasma center).

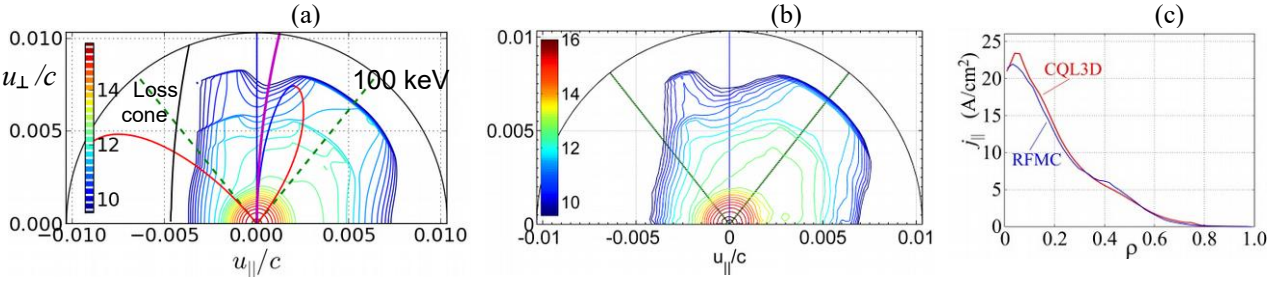

FIGURE 4. Steady-state distribution functions for NBI in NSTX at the midplane position R=126cm: (a) from CQL3D run, and (b) RFMC run. Also, (c) compares the profiles of current density calculated with the two codes. Dashed lines indicate ZOW trapped-passing boundaries (just for reference), and solid lines in (a) are FOW-type boundaries (see [2] for details).

It is seen that the features of FI deposition, pitch angle scattering, and slowing down are very much alike in the two codes. The profiles of flux-surface-average current density, shown in Fig. 4(c), are nearly the same in the CQL3D-FOW and RFMC-FOW runs; they are broader than in corresponding ZOW runs (not shown here). We have not yet applied RF heating in this test – the fast ions could gain a substantial energy beyond initial injection energy from HHFW because of finite Larmor radius effects. The preparations for such tests are underway, and we also plan to compare our results with NUBEAM+TORIC calculations.

ACKNOWLEDGMENTS

The work is supported by USDOE grants ER54649, ER54744, and DE-SC0018090. The authors acknowledge Drs. N. Bertelli, P. T. Bonoli, D. L. Green, D. N. Smithe, J. C. Wright and the RF-SciDAC group for helpful discussions.

REFERENCES

1. R.W. Harvey and M. McCoy, "The CQL3D Fokker Planck Code", www.compxco.com/cql3d.html
2. Yu.V. Petrov and R.W. Harvey, *Plasma Phys. Control. Fusion* **58**, 115001 (2016).
3. R.W. Harvey, D.K. Bhadra, and S.C. Chiu, "Calculations of Neutral Beam Power Deposition for Doublet III", Poster 3B5, Sherwood Theory Meeting, Tuscon, 1980. Also www.compxco.com/mcgo.html
4. R. W. Harvey, Yu. V. Petrov, C. C. Kim, et al., "Time-Dependent Runaway Electron Simulations: Ampere-Faraday Equations implemented in CQL3D", *Nucl. Fusion*, in press (2019). https://doi.org/10.1088/1741-4326/ab38cb
5. T. H. Stix, *Nucl. Fusion* **15**, 737 (1975).
6. X. Q. Xu and M. N. Rosenbluth, *Phys. Fluids B* **3**, 627 (1991).
7. J. H. Kwon, et al., *Bull. Amer. Phys. Soc. (DPP)* **48**, poster VP1.00115 (2006).
8. N. Bertelli, et al., EPJ Web of Conferences **157**, 03004 (2017).

9. G. D. Kerbel and M. G. McCoy, *Phys. Fluids* **28**, 3629 (1985).
10. M. A. Kovanen, W. G. F. Core, and T. Hellsten, *Nucl. Fusion* **5**, 787 (1992).
11. R.W. Harvey, Yu.V. Petrov, E.F. Jaeger, P.T. Bonoli, A. Bader, and RF-SciDAC Group, "Differences Between QL and Exact Ion Cyclotron Resonant Diffusion", paper TH/P6-08, Proc. of IAEA FEC 2012, San Diego, CA.